### Design and Analysis of Multifunctional Metasurface for Linear and Circular Polarized Incident Wave

Sylvie RANA <sup>1,2</sup>, Samiran PRAMANIK <sup>1,3</sup>, Debasis MITRA <sup>1</sup>, Chaitali KOLEY <sup>3</sup>

<sup>3</sup> Dept. of Electronics and Communication Engineering, National Institute of Technology, Mizoram, India

sylvierana21@iitk.ac.in

Submitted February 19, 2025 / Accepted August 5, 2025 / Online first October 24, 2025

**Abstract.** A passive multifunctional metasurface design has been proposed in this work for both linear and circular polarized incidences, between a frequency range of 4-7 GHz. The proposed unit cell structure comprises of concentric split pentagonal rings, loaded with two lumped capacitors on the top layer, having single dielectric layer. The main functionalities include polarization selective absorption (4.31–4.36 GHz) and reflective cross-polarization conversion (5.79–6.02 GHz) for linear polarized incidences. Moreover, polarization handedness maintaining reflection (4.57–5.45 GHz) and polarization selective absorption (6.12–6.26 GHz) for circular polarized incidences has been achieved. A sample prototype of 10 × 10-unit cells ( $2\lambda_0 \times 2\lambda_0$ ), was fabricated and the experimental results were verified with the simulated ones. Since the proposed design has such diversified functionalities for both linear and circular polarized incidences, it can find probable applications in polarimetric imaging techniques, polarization modulation devices, polarization sensors etc.

#### **Keywords**

Lumped capacitor, multifunctional metasurface, polarization converter, polarization selective absorber

#### 1. Introduction

In the last few years, metasurface based devices have gained huge dominance in engineering due to its unique ability to manipulate the electromagnetic (EM) waves and versatile applicability [1] in various areas like negative refraction [2], independent control of reflection [3], EM scatterer [4], microwave absorption [5–7], polarization conversion and manipulation [8–10], etc.

In the past, metasurfaces have been substantially applied for linear polarized (LP) absorption (LP-A) [11–15] as well as circular polarized (CP) absorption (CP-A) [16–19]. Besides, linear to linear orthogonal polarization conversion (LP-LP) [20–22] and circular to circular polarization hand-

edness maintaining (CP-CP) [23], [24] reflection, were also explored predominantly among the other kinds of reflective polarization converters (PCs). Naturally, such PCs found extensive use in RCS reduction [25], antennae with polarization reconfigurable facilities [26], microwave measurement, and polarization manipulation and control devices [27]. However, these reported designs have been developed mainly for single functionality and thus fail to meet growing demands of devices having multiple functions.

To mitigate this problem, reconfigurable or switchable metasurfaces, using PIN diodes were reported [28–32]. They offered multi-functionalities like LP-A and LP-LP for LP incidences. In the meantime, switchable metasurfaces were designed both with [28], [29] and without [30], [31] air spacers apart from a dielectric layer, where the operating modes could be selected by switching the state of PIN diodes. Li et. al [28], reported LP-LP and LP-A when the diode was in ON and OFF states respectively. Similar phenomenon was noted in [29] and [30], but conversion and absorption were achieved for ON and OFF states of the diodes respectively. In [31], absorption and conversion modes were achieved with varactor diode. Again, multi-functionality was achieved by switching between frequency bands with LP-LP functionality, as reported in [33]. LP-CP conversion along with LP-LP was also achieved by four PIN diodes in [34]. Although, these designs exhibited more than one functionality by integrating the PIN diodes or varactor diodes, they introduced complex biasing arrangement with higher loss due to active elements [28]. Moreover, all of them were appropriate mainly for LP incidences and inconvenient for CP incidences.

To overcome these issues, passive multifunctional devices, based on metasurface were introduced [35–40], where they could simultaneously manipulate the state of LP and CP incidence waves. In [24, 41, 42], according to the incident polarization, the operating mode could be chosen from LP-LP and CP-CP. These reported passive multifunctional metasurfaces only work in polarization conversion mode but not in absorption mode. However, LP-LP, CP-CP, LP-A, and CP-A, all modes are equally demanding for various EM applications [11, 15, 17]. Recently, multifunctionality has

DOI: 10.13164/re.2025.0575

<sup>&</sup>lt;sup>1</sup> Dept. of Electronics and Telecommunication, Indian Institute of Engineering Science and Technology, Shibpur, India 

<sup>2</sup> Dept. of Electrical Engineering, Indian Institute of Technology, Kanpur, India

been demonstrated with devices achieving LP-LP and LP-A conversions as shown in [43], and trifunctionality encompassing LP-LP, LP-CP, and LP-A conversions as reported in [44]. However, to the best of our knowledge, no device has yet been reported that can simultaneously realize LP-LP and LP-A states under linearly polarized (LP) incidence, as well as CP-CP and CP-A states under circularly polarized (CP) incidence.

In this paper, we have introduced a single-substrate layered, multifunctional passive metasurface based on concentric split pentagonal geometry embedded with lumped capacitors. Unlike previously reported devices, the proposed design has the unique ability to behave as both absorber and polarization converter simultaneously for both LP and CP incidences. The proposed device offers LP-A under x-polarized incidence, in addition to LP-LP under both x-polarized and y-polarized incidences. Moreover, it also offers CP-A for lefthanded circular polarized (LCP) incidence, along with CP-CP for both LCP and right-handed circular polarized (RCP) incidences. It is noteworthy to mention that the handedness of circular polarization mentioned throughout this paper has been considered with respect to +z-axis. Further, we have elucidated its working mechanism, with the heLP of the surface current density and distribution analysis of the proposed device. Finally, the proposed device is fabricated, and measurements were carried out to confirm the working principle. The proposed structure maybe be applied for environments where handedness-maintained CP reflection is required like satellite communication [39], [40], satellite TV [41], deep space missions [42], [43] etc., along with areas like stealth where out of band absorption of a particular polarized wave is required [44]. The proposed structure can easily be scaled to accommodate other applications that match the proposed functionalities due to its simple structure.

## 2. Design and Analysis of Proposed Multifunctional Structure

#### 2.1 Geometrical Configuration

The proposed unit cell structure is shown in Fig. 1(a), where the unit cell can be broken down into three distinct parts: 1) top patterned patch, 2) middle dielectric and 3) bottom continuous ground. The top part consisting of two concentric pentagonal strips of different size, having two splits on two of their sides were printed on FR4 substrate ( $\varepsilon_{\rm r}=4.3$ , and  $\tan\delta=0.025$ ) with thickness of 2.8 mm. One of the sides containing the gaps have been filled with two lumped capacitors ( $C=0.1\,{\rm pF}$ ) to match the free space impedance. The back side of substrate is laminated by copper ground plane to avoid transmission of EM wave through the surface. The dimensions used here are given as: ( $a=14\,{\rm mm}, p_1=4.5\,{\rm mm}, p_2=6\,{\rm mm}, g_1=g_2=1.8\,{\rm mm}, w=1\,{\rm mm}, h=2.8\,{\rm mm}, t=0.035\,{\rm mm}$ ).

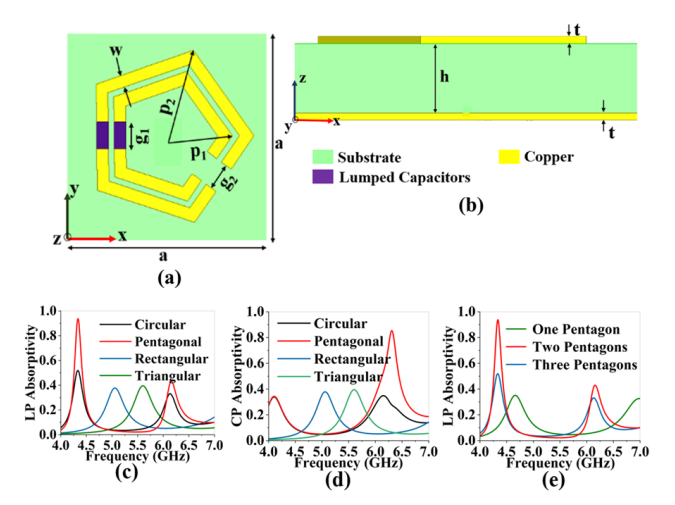


**Fig. 1.** Schematic representation of proposed multifunctional metasurface. (a) Top view; (b) side view of the unit cell; (c) and (d) effect of shape of strips on LP and CP absorptivity respectively; (e) effect of number of parallel strips on LP absorptivity.

The pentagonal geometry in our structure was chosen to introduce diagonal asymmetry, unlike even-sided shapes (e.g., square, hexagon, octagon) that exhibit diagonal symmetry and thus suppress chiral responses critical for polarization conversion and polarization-sensitive absorption. The inherent asymmetry of the pentagon enhances chiral behavior, as shown in Fig. 1(c) and (d). Further, the slits in the pentagonal rings disrupt mirror symmetries of the metallic surface's n-fold rotational symmetry, reinforcing polarization conversion. Figure 1(e) shows that configurations with a single or triple ring result in weaker resonances and absorption, however with two rings, strong absorption, following the well-known double split ring resonator (DSRR) design principles.

#### 2.2 Simulated Reflection Coefficients

The proposed unit cell is simulated in CST Microwave Studio using Floquet ports and master-slave boundaries. For linearly polarized (LP) y-incidence, the co-polarized and cross-polarized reflection coefficients are defined as  $R_{yy} = \frac{|\vec{E}_y^r|}{|\vec{E}_y^r|}$  and  $R_{xy} = \frac{|\vec{E}_x^r|}{|\vec{E}_y^r|}$ , respectively. For circularly polarized (CP) incidence, the corresponding coefficients are  $R_{LL} = \frac{|\vec{E}_y^r|}{|\vec{E}_z^r|}$  and  $R_{RL} = \frac{|\vec{E}_R^r|}{|\vec{E}_L^r|}$ . Here, superscripts r and i denote reflected and incident fields, respectively. Similar definitions apply for x-polarized and RCP incidences. Figure 2 presents the simulated reflection responses under normal incidence. For x-polarization (see Fig. 2(a)),  $R_{xx}$  and  $R_{yx}$  remain below  $-10\,\mathrm{dB}$  in the  $4.31-4.36\,\mathrm{GHz}$  band, indicating strong absorption. In the  $5.87-5.98\,\mathrm{GHz}$  band,  $R_{xx}$  stays below  $-8\,\mathrm{dB}$ , while  $R_{yx}$  exceeds  $-3\,\mathrm{dB}$ , confirming polarization conversion.

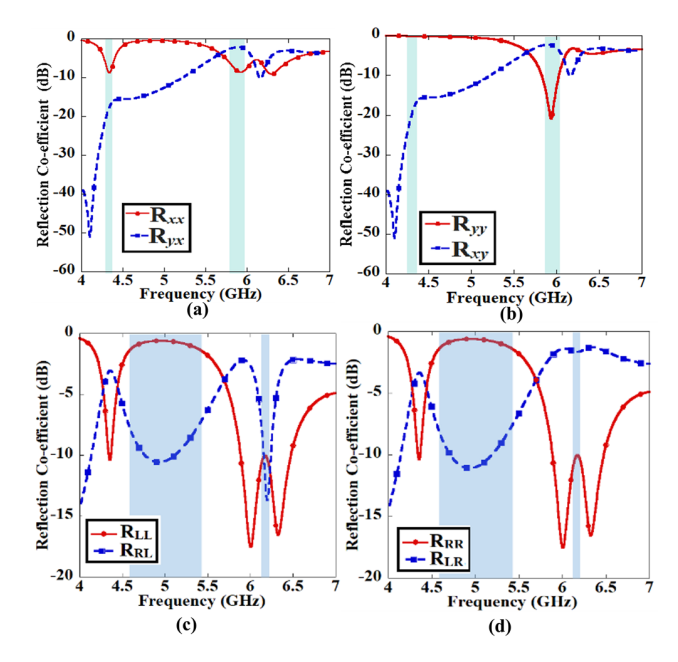


Fig. 2. Simulation results of co and cross-polarized reflection coefficients under (a) x-polarized, (b) y-polarized, (c) LCP, and (d) RCP incidences.

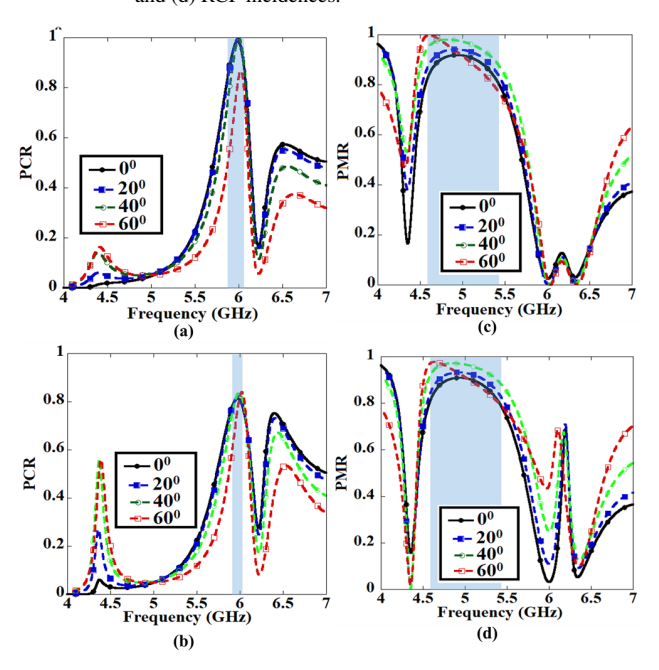
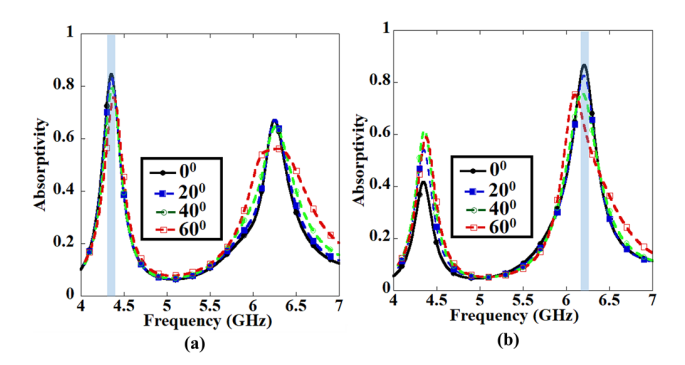


Fig. 3. Simulation results of PCR with incident angle  $(\theta)$  variation under (a) x-polarized, (b) y-polarized LP incidences and of PMR for (c) LCP and (d) RCP incidences.

#### 3. Mechanism from Surface Currents

For y-polarization (Fig. 2(b)),  $R_{yy}$  is above -3 dB and  $R_{xy}$  is below -10 dB in the lower band, while in the higher band (5.79–6.05 GHz),  $R_{yy}$  drops below -8 dB and  $R_{xy}$  exceeds -3 dB. For CP incidence (Figs. 2(c)–(d)), both  $R_{LL}$  and  $R_{RR}$  remain above -1.5 dB and  $R_{RL}$ ,  $R_{LR}$  stay below -8 dB across 4.57–5.45 GHz, indicating handedness preservation. In the 6.16–6.26 GHz range,  $R_{LL}$  and  $R_{RL}$  fall below -10 dB under LCP incidence, implying strong absorption.



**Fig. 4.** Simulation results of absorptivity with incident angle  $(\theta)$  variation for (a) x-polarized LP and (b) LCP incidences.

Conversely, for RCP incidence,  $R_{RR}$  drops below -8 dB and  $R_{LR}$  exceeds -3 dB, resembling metallic reflection behavior.

#### 3.1 Performance Analysis

To evaluate the effectiveness of the proposed unit cell, polarization conversion ratio (PCR) for LP-LP and polarization handedness maintaining ratio (PMR) for CP-CP, along with linear and circular absorptivity, are computed under oblique incidence. For LP and CP cases, PCR [26] and PMR [23] are defined as:

$$PCR = \frac{|R_{cross-pol}|^2}{|R_{cross-pol}|^2 + |R_{co-pol}|^2},$$
 (1)

$$PMR = \frac{|R_{\text{co-pol}}|^2}{|R_{\text{cross-pol}}|^2 + |R_{\text{co-pol}}|^2}.$$
 (2)

As shown in Fig. 3, the PCR exceeds 0.8 in the  $5.87-5.98\,\text{GHz}$  band for x-polarization (Fig. 3(a)) and  $5.79-6.05\,\text{GHz}$  for y-polarization (Fig. 3(b)), sustaining performance up to  $60^\circ$  incidence. Similarly, the PMR remains above 0.8 across  $4.56-5.43\,\text{GHz}$  for both LCP and RCP, validating CP-CP behavior, though it declines at angles beyond  $60^\circ$ .

Absorptivity (A) for both LP [15] and CP [19] incidences is calculated as:

$$A = 1 - |R_{\text{co-pol}}|^2 - |R_{\text{cross-pol}}|^2.$$
 (3)

For x-polarized incidence, *A* exceeds 0.8 in the 4.31–4.36 GHz range and remains stable across oblique angles (Fig. 4(a)). In contrast, absorptivity for y-polarization is below 0.02 in the same band, indicating x-polarization selective absorption. For LCP incidence, absorptivity exceeds 0.8 in the 6.12–6.22 GHz band up to 60° (Fig. 4(b)), whereas RCP absorption remains below 0.25, demonstrating selectivity. Absorption peaks observed at 6.13–6.25 GHz (x-polarization) and 4.34 GHz (LCP/RCP) are excluded due to poor absorptivity. A summary of the key polarization behaviors is provided in Tab. 1.

Incident polarization	Frequency [GHz]	Function	Remarks
Linear	4.31 – 4.36	x-LP absorption	A > 0.8
	5.79 – 6.02	Orthogonal polarization conversion for both x- and y-polarized wave	PCR > 0.8
Circular	4.57 – 5.43	Polarization handedness keeping reflection for both LCP and RCP	PMR > 0.8
Circulai	6.12 - 6.26	LCP selective absorption	A > 0.8

Note: A: Absorptivity; PCR: Polarization conversion ratio; PMR: Polarization handedness maintaining ratio.

Tab. 1. Summary of polarization-dependent functions.

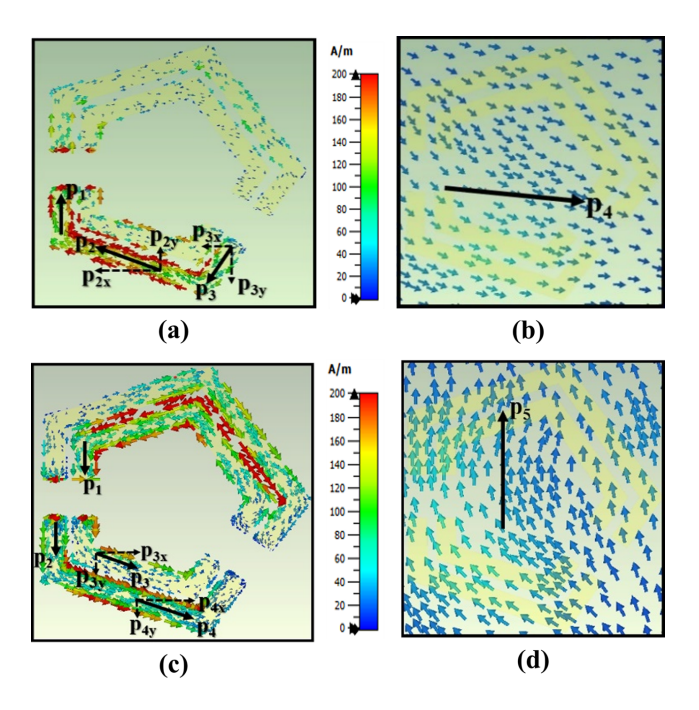


Fig. 5. Current distribution of (a) top layer and (b) bottom layer for x-polarized incidence, and (c) top layer and (d) bottom layer for y-polarized incidence of the proposed structure.

#### 3.2 Polarization Conversion for LP Incidence

The surface current distribution for various polarized incidences is analyzed to understand the mechanism of multifunctionality. As shown in Fig. 5, the induced electric moments (**p**) on the top layer are primarily concentrated on the lower part of the pentagonal structures. Decomposing them into x- and y-components, Figure 5(a) reveals that  $\mathbf{p}_{2x}$  and  $\mathbf{p}_{3x}$  are in phase, while the antiparallel moment  $\mathbf{p}_4$  shown in Fig. 5(b) on the ground layer leads to magnetic resonance. Meanwhile, the y-components  $\mathbf{p}_{2y}$  and  $\mathbf{p}_{3y}$  cancel each other, while  $\mathbf{p}_1$  contributes entirely to reflection, making y-polarized reflection dominant for x-polarized incidence.

For y-polarized incidence, as seen in Fig. 5(c), the y-components  $\mathbf{p}_1$ ,  $\mathbf{p}_2$ ,  $\mathbf{p}_{3y}$ , and  $\mathbf{p}_{4y}$  align and add up, while the opposing  $\mathbf{p}_5$  in the ground layer generates magnetic resonance. Simultaneously, the x-components  $\mathbf{p}_{3x}$  and  $\mathbf{p}_{4x}$  contribute to radiation, leading to x-polarized reflection. Although strong currents appear on the upper portion of the pentagonal strips for x-polarized incidence, their opposing directions cause cancellation of moments, preventing their participation in reflection.

#### 3.3 Surface Current Density for CP Incidence

For CP incidence, the current distributions in the conductive layers are analyzed by decomposing them into x- and y-components [45]. The reflected wave along the +z-axis can be expressed as:

$$\hat{E}_{x} = E_{m} e^{j\phi_{x}}, \quad \hat{E}_{y} = E_{m} e^{j\phi_{y}}.$$

The handedness of the reflected wave is determined by the phase difference  $\phi_y - \phi_x$ , where  $\phi_y - \phi_x = +90^\circ$  for LCP and  $\phi_y - \phi_x = -90^\circ$  for RCP. Figure 6(a) and Figure 6(b) illustrate the x- and y-components of induced currents under LCP illumination at 5 GHz. The x-component is primarily concentrated on the top layer, while the bottom layer contributes to the y-component. The radiation from the y-component experiences a path phase shift of  $-\beta z$ , calculated as  $-34.88^\circ$  for a dielectric constant of 4.3 and a height of 2.8 mm. From Fig. 6(b), the y-component phase at the bottom layer is  $120^\circ$ , and from Fig. 6(a), the x-component phase ( $\phi_x$ ) is  $0^\circ$ . Thus, the phase at the top layer is:  $\phi_y = 120^\circ - 34.88^\circ = 85.12^\circ$  yielding  $\phi_y - \phi_x = 85.12^\circ$  which is close to  $+90^\circ$ , confirming LCP reflection for LCP incidence.

Similarly, for RCP incidence at 5 GHz, the x-component of the induced current is primarily concentrated on the top layer, as shown in Fig. 6(c), with a phase ( $\phi_x$ ) of 180°. Meanwhile, the y-component is dominant on the bottom layer, as depicted in Fig. 6(d), with a maximum phase of 120°. As the y-component propagates to the top layer, its phase reduces to 85.12°, resulting in: ( $\phi_y - \phi_x = 85.12^\circ - 180^\circ = -84.88^\circ$ ) which approximates to  $-90^\circ$ , confirming RCP reflection for RCP incidence.

#### 3.4 Mechanism of Absorption

The absorption mechanism is analyzed based on the induced current distribution on the top layer, as shown in Fig. 7. For x-polarized LP incidence, strong currents are concentrated on the outer pentagonal loop at the absorption peak of 4.34 GHz, as seen in Fig. 7(a). Due to capacitive effects, the inner loop also exhibits strong currents at its edge facing the outer loop, generating electric resonance which enhances absorption. Similarly, for LCP incidence, an absorption peak at 6.18 GHz is observed, attributed to strong currents on the top layer, as depicted in Fig. 7(b). The inner loop also shows current distribution, while capacitive effects induce additional currents on the outer loop, leading to strong electric resonance and effective absorption of LCP waves.

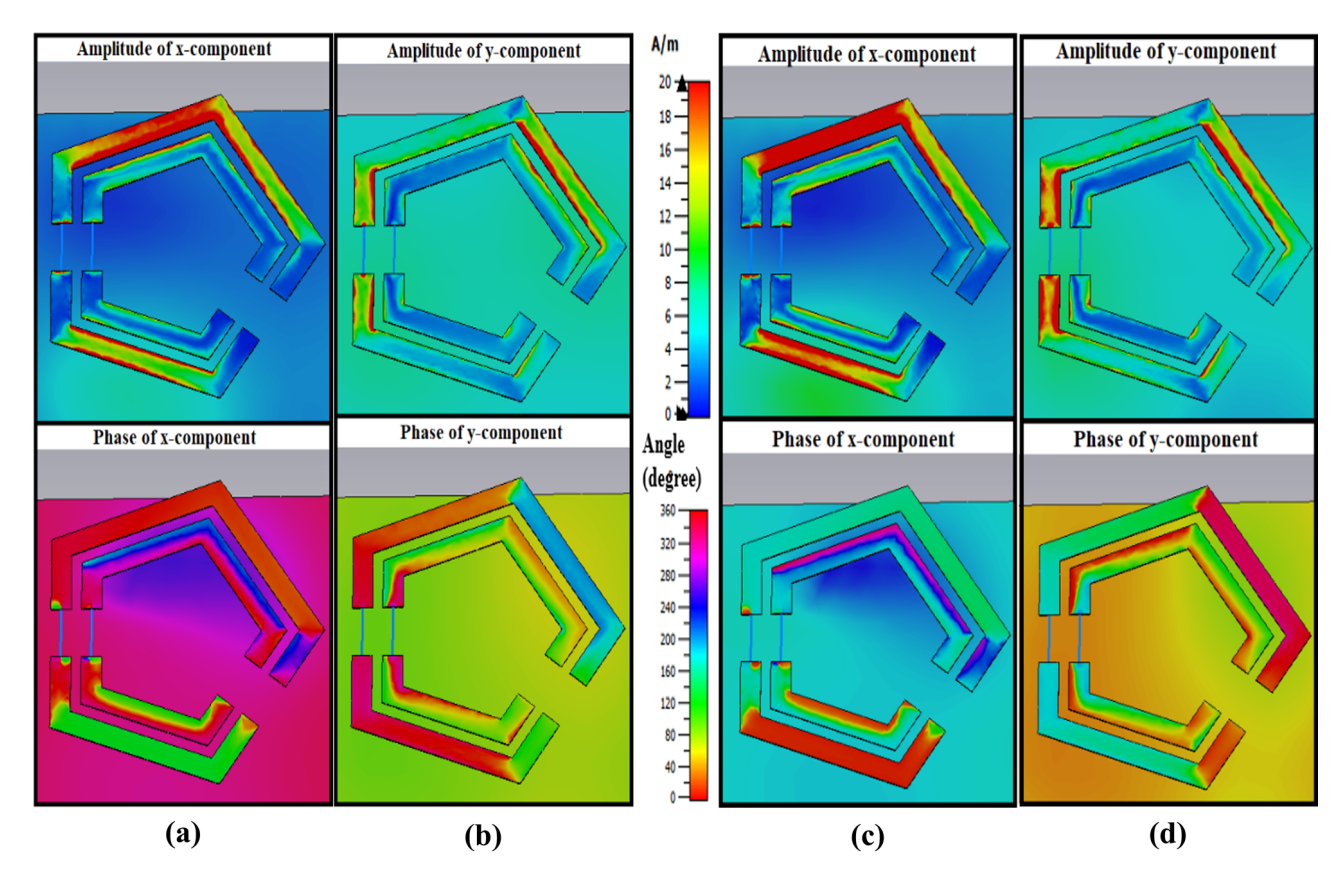


Fig. 6. Amplitude and phase of (a) x-component, and (b) y-component for LCP incidence; (c) x-component, and (d) y-component for RCP incidence, of the surface current distribution on top and bottom layers of the proposed structure at 5 GHz.

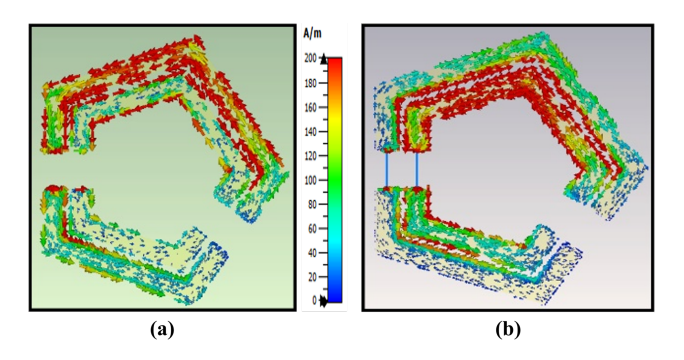


Fig. 7. Current distributions on top layer for (a) x-polarized incidence at 4.34 GHz and (b) LCP incidence at 6.18 GHz.

# (a) (b)

**Fig. 8.** (a) Top view of fabricated sample and (b) experimental setup.

#### 4. Fabrication and Measurement

A prototype sample was fabricated, as shown in Fig. 8(a), by using printed circuit board (PCB) technique, having  $10 \times 10$ -unit cells. The lumped capacitors (VJ0805 SMD Multilayer Ceramic Capacitor) were used on the PCB.

The fabricated sample was measured using the free-space method in front of an anechoic chamber wall, as shown in Fig. 8(b). Two wideband horn antennas (transmitter and receiver) were positioned 1 m from the sample and connected to an Anritsu MS2038C network analyzer to measure co- and cross-polarized reflection magnitudes. Calibration was performed using a copper plate of the same dimensions before testing the prototype.

The measured reflection magnitudes confirmed LP-LP conversion in the 5.87–5.98 GHz range for x-polarized incidence and 5.79–6.02 GHz for y-polarized incidence, as seen in Fig. 9(a) and (b). The LP-LP bandwidth for x-polarized incidence was slightly larger than for y-polarized, consistent with earlier observations. Additionally, LP-A was observed at 4.31–4.36 GHz for x-polarized waves. For CP incidence, CP-CP conversion occurred in the 4.57–5.45 GHz range, as shown in Fig. 9(c) and (d). At higher frequencies (6.15–6.26 GHz), the sample exhibited CP-A for LCP and handedness-reversed reflection for RCP. The experimental results closely matched simulations, with minor deviations due to ripples, fabrication tolerances, and SMD component uncertainties.

Ref.	Absorption		LP-LP	СР-СР	LP-CP	Unit cell geometry	Lumped elements		Unit cell	Prof.	No. of
	LP	CP					Active	Passive	$(\lambda_0 \times \lambda_0)$	$(\lambda_0)$	func.
[28]	<b>√</b>	-	✓	-	_	Cross loop	PIN	R	$0.34 \times 0.34$	0.150	2
[29]	<b>√</b>	-	✓	-	-	Fish-bone structure	PIN	R	$0.26 \times 0.26$	0.048	2
[31]	<b>√</b>	-	✓	-	-	Square ring + patch	Varicap	_	$0.30 \times 0.30$	0.020	2
[33]	-	-	✓	-	-	Square double slotted rings	PIN	L	$0.20 \times 0.20$	0.056	2
[34]	-	-	✓	-	✓	Arrow patch + square island	PIN	-	$0.35 \times 0.35$	0.019	2
[36]	_	-	✓	✓	_	Truncated patch	-	_	0.44 × 0.44	0.074	2
[41]	_	-	✓	-	✓	Split ring loaded cross dipole	-	-	$0.4 \times 0.4$	0.95	2
[42]	_	-	✓	✓	✓	Cross slot	_	-	0.14 × 0.13	0.034	2
[44]	<b>√</b>	-	✓	-	✓	Split ring + L-shaped strip	_	-	0.25 × 0.25	0.071	3
Our work	<b>√</b>	✓	✓	✓	_	Double pentagonal slotted rings	-	С	0.20 × 0.20	0.040	4

Note: R: resistor; L: inductor; C: capacitor.

Tab. 2. Comparison of reported multifunctional metasurfaces.

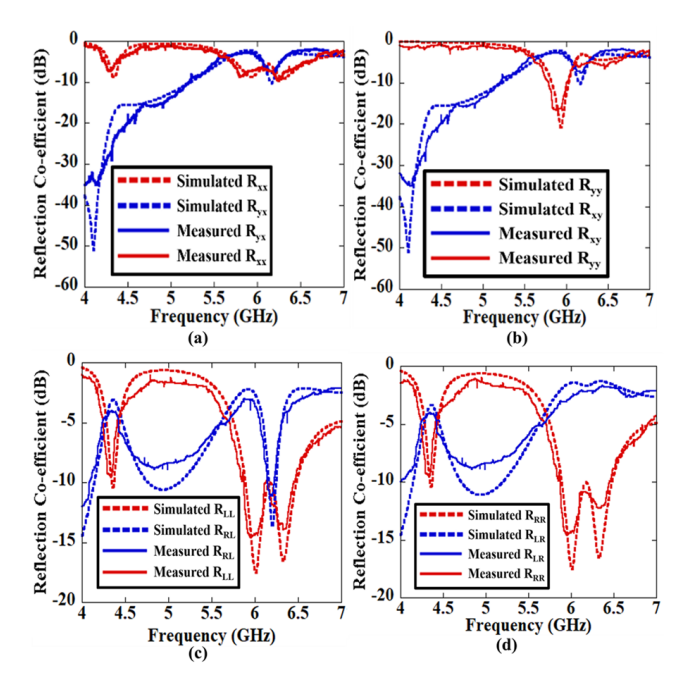


Fig. 9. Simulated and measurement results of fabricated sample under (a) x-polarized, (b) y-polarized incident LP wave, (c) LCP and (d) RCP incident wave.

This work demonstrates a multifunctional metasurface with a higher number of functionalities and a relatively thinner substrate, as summarized in Tab. 2. The substrate thickness and unit cell dimensions are normalized to  $\lambda_0$ , the highest resonant wavelength.

#### 5. Conclusion

A passive multifunctional metasurface has been designed by using a simple concentric spilt pentagonal structure, having a single dielectric layer. The polarization selective absorption was found for both linear and circular polarized incidences at lower and higher frequency bands

respectively. At the same time, cross-polarized reflection and polarization handedness keeping reflection was found for linear and circular polarized incidences respectively. The ability to provide functionality for both linear and circular polarized incidences with a simple top layer design, without any active elements and having single dielectric layer are the main advantages of this work. Presence of these qualities may enable this work to be suitable for applications like polarimetric imaging, polarization modulations, polarization sensors, satellite communications etc.

#### Acknowledgments

This work acknowledges research project funded by the Indian Institute of Technology Guwahati Technology Innovation and Development Foundation (IITG TI & DF), DST, Govt. of India, under the grant TIH/TD/0303.

#### References

- [1] HOLLOWAY, C., KUESTER, E., GORDON, J., et al. An overview of the theory and applications of metasurfaces: The two-dimensional equivalents of metamaterials. *IEEE Antennas* and Propagation Magazine, 2012, vol. 54, no. 2, p. 10–35. DOI: 10.1109/MAP.2012.6230714
- [2] PENDRY, J. A chiral route to negative refraction. Science, 2004, vol. 306, no. 5700, p. 1353–1354. DOI: 10.1126/science.1104467
- [3] MA, H., WANG, G., KONG, G., et al. Independent controls of differently-polarized reflected waves by anisotropic metasurfaces. *Scientific Reports*, 2015, vol. 5, p. 1–6. DOI: 10.1038/srep09605
- [4] MODI, A., BALANIS, C., BIRTCHER, C., et al. Novel design of ultrabroadband radar cross section reduction surfaces using artificial magnetic conductors. *IEEE Transactions on Antennas and Propagation*, 2017, vol. 65, no. 10, p. 5406–5417. DOI: 10.1109/TAP.2017.2734069

- [5] ZHANG, C., CHENG, Q., YANG, J., et al. Broadband metamaterial for optical transparency and microwave absorption. *Applied Physics Letters*, 2017, vol. 110, no. 14, p. 1–5. DOI: 10.1063/1.4979543
- [6] CHENG, Y., LUO, H., CHEN, F., et al. Broadband metamaterial microwave absorber based on asymmetric sectional resonator structures. *Applied Physics Letters*, 2020, vol. 127, no. 21, p. 1–7. DOI: 10.1063/5.0002931
- [7] PANG, Y., SHEN, Y., LI, Y., et al. Water-based metamaterial absorbers for optical transparency and broadband microwave absorption. *Applied Physics Letters*, 2018, vol. 123, no. 15, p. 1–5. DOI: 10.1063/1.5023778
- [8] SONG, S., MA, X., PU, M., et al. Tunable multiband polarization conversion and manipulation in vanadium dioxide-based asymmetric chiral metamaterial. *Applied Physics Express*, 2018, vol. 11, no. 4, p. 1–4. DOI: 10.7567/APEX.11.042004
- [9] DONG, G., QIN, C., LV, T., et al. Dynamic chiroptical responses in transmissive metamaterial using phase-change material. *Journal of Physics D: Applied Physics*, 2020, vol. 53, no. 28, p. 1–9. DOI: 10.1088/1361-6463/ab8516
- [10] ZHU, B., FENG, Y., ZHAO, J., et al. Polarization modulation by tunable electromagnetic metamaterial reflector/absorber. *Optics Express*, 2010, vol. 18, no. 22, p. 23196–23202. DOI: 10.1364/OE.18.023196
- [11] BASKEY, H. B., JOHARI, E., AKHTAR, M. J., et al. Metamaterial structure integrated with a dielectric absorber for wideband reduction of antennas radar cross section. *IEEE Transactions* on *Electromagnetic Compatibility*, 2017, vol. 59, no. 4, p. 1–10. DOI: 10.1109/TEMC.2016.2639060
- [12] SHARMA, S. K., GHOSH, S., SRIVASTAVA, K. V., et al. An ultrathin triple-band polarization-insensitive metamaterial absorber for S, C and X band applications. *Applied Physics A*, 2016, vol. 122, p. 1–8. DOI: 10.1007/s00339-016-0588-4
- [13] SINGH, A. K., ABEGAONKAR, M. P., KOUL, S. K., et al. A triple band polarization insensitive ultrathin metamaterial absorber for S-, C-, and X-bands. *Progress In Electromagnetics Research M*, 2019, vol. 77, p. 187–197. DOI: 10.2528/PIERM19011802
- [14] PAQUAY, M., IRIARTE, J. C., EDERRA, I., et al. Thin AMC structure for radar cross-section reduction. *IEEE Transactions* on Antennas and Propagation, 2007, vol. 55, no. 12, p. 1–9. DOI: 10.1109/TAP.2007.910306
- [15] ZUO, P., LI, T., WANG, M., et al. Miniaturized polarization insensitive metamaterial absorber applied on EMI suppression. *IEEE Access*, 2019, vol. 8, p. 6583–6590. DOI: 10.1109/ACCESS.2019.2957308
- [16] STOJANOVIC, D. B., GLIGORIC, G., BELICEV, P. P., et al. Circular polarization selective metamaterial absorber in terahertz frequency range. *IEEE Journal of Selected Topics in Quantum Electronics*, 2021, vol. 27, no. 1, p. 1–6. DOI: 10.1109/JSTQE.2020.3024570
- [17] PAN, M., LI, Q., HONG, Y., et al. Circular-polarization-sensitive absorption in refractory metamaterials composed of molybdenum zigzag arrays. *Optics Express*, 2018, vol. 26, no. 14, p. 17772, p. 1–9. DOI: 10.1364/OE.26.017772
- [18] JING, L., WANG, Z., YANG, Y., et al. Chiral metamirrors for broadband spin-selective absorption. *Applied Physics Letters*, 2017, vol. 110, no. 23, p. 1–7. DOI: 10.1063/1.4985132
- [19] TANG, B., LI, Z., PALACIOS, E., et al. Chiral-selective plasmonic metasurface absorbers operating at visible frequencies. *IEEE Photonics Technology Letters*, 2017, vol. 29, no. 3, p. 295–298. DOI: 10.1109/LPT.2016.2647262

- [20] FU, C., SUN, Z., HAN, L., et al. Dual-bandwidth linear polarization converter based on anisotropic metasurface. *IEEE Photonics Journal*, 2020, vol. 12, no. 2, p. 1–11. DOI: 10.1109/JPHOT.2019.2962336
- [21] IBRAHIM, M. S., MAHMOUD, A., AWAMRY, A., et al. Wideband anisotropic unit cell design for perfect cross-polarization conversion. *IEEE International Symposium on Antennas and Propagation USNC-URSI Radio Science Meeting*. Atlanta (GA, USA), 2019, p. 1–2. DOI: 10.1109/APUSNCURSINRSM.2019.8889282
- [22] AKO, R. T., LEE, W. S. L., BHASKARAN, M., et al. Broad-band and wide-angle reflective linear polarization converter for terahertz waves. APL Photonics, 2019, vol. 4, no. 9, p. 96104–96110.DOI: 10.1063/1.5116149
- [23] HUANG, X., CHEN, J., YANG, H., et al. High-efficiency wideband reflection polarization conversion metasurface for circularly polarized waves. *Journal of Applied Physics*, 2017, vol. 122, no. 4, p. 1–4. DOI: 10.1063/1.4996643
- [24] YANG, D., LIN, H., HUANG, X., et al. Dual broadband metamaterial polarization converter in microwave regime. *Progress In Electromagnetics Research Letters*, 2016, vol. 61, p. 71–76. DOI: 10.2528/PIERL16033004
- [25] LIU, Y., HAO, Y., LI, K., et al. Radar cross section reduction of a microstrip antenna based on polarization conversion metamaterial. *IEEE Antennas and Wireless Propagation Letters*, 2015, vol. 15, p. 80–83. DOI: 10.1109/LAWP.2015.2430363
- [26] BAKSHI, S. C., MITRA, D., GHOSH, S., et al. A frequency selective surface based reconfigurable rasorber with switchable transmission/reflection band. *IEEE Antennas and Wireless Propagation Letters*, 2021, vol. 18, no. 1, p. 29–33. DOI: 10.1109/LAWP.2018.2878858
- [27] LIN, B., GUO, J., CHU, P., et al. Multiple-band linear-polarization conversion and circular polarization in reflection mode using a symmetric anisotropic metasurface. *Physical Review Applied*, 2018, vol. 9, no. 2, p. 1–10. DOI: 10.1103/PhysRevApplied.9.024038
- [28] LI, Y., LI, H., WANG, Y., et al. A novel switchable absorber/linear converter based on active metasurface and its application. *IEEE Transactions on Antennas and Propagation*, 2020, vol. 68, no. 11, p. 7688–7693. DOI: 10.1109/TAP.2020.2980301
- [29] WANG, J., YANG, R., MA, R., et al. Reconfigurable multifunctional metasurface for broadband polarization conversion and perfect absorption. *IEEE Access*, 2020, vol. 8, p. 105815–105823. DOI: 10.1109/ACCESS.2020.3000042
- [30] DUTTA, R., MITRA, D., GHOSH, J., et al. Dual-band multifunctional metasurface for absorption and polarization conversion. *Inter*national Journal of RF and Microwave Computer-Aided Engineering, 2020, vol. 30, no. 7, p. 1–7. DOI: 10.1002/mmce.22200
- [31] HA, D. T., DZUNG, D. N., NGOC, N. V., et al. Switching between perfect absorption and polarization conversion, based on hybrid metamaterial in the GHz and THz bands. *Journal of Physics D: Applied Physics*, 2021, vol. 54, no. 23, p. 1–11. DOI: 10.1088/1361-6463/abeb97
- [32] PITILAKIS, A., TSILIPAKOS, O., LIU, F., et al. A multi-functional reconfigurable metasurface: Electromagnetic design accounting for fabrication aspects. *IEEE Transactions on Antennas and Propagation*, 2021, vol. 69, no. 3, p. 1440–1454. DOI: 10.1109/TAP.2020.3016479

- [33] SUN, S., JIANG, W., GONG, S., et al. Reconfigurable linear-to-linear polarization conversion metasurface based on PIN diodes. *IEEE Antennas and Wireless Propagation Letters*, 2018, vol. 17, no. 9, p. 1722–1726. DOI: 10.1109/LAWP.2018.2864797
- [34] YANG, X., WEN, E., BHARADIA, D., et al. Multifunctional metasurface: Simultaneous beam steering, polarization conversion, and phase offset. *IEEE Transactions on Antennas and Propagation*, 2024, vol. 72, no. 5, p. 4589–4593. DOI: 10.1109/TAP.2024.3371697
- [35] POUYANFAR, N., NOURINIA, J., GHOBADI, C., et al. Multi-band and multifunctional polarization converter using an asymmetric metasurface. *Scientific Reports*, 2021, vol. 11, p. 1–15. DOI: 10.1038/s41598-021-88771-x
- [36] LI, L., LI, Y., WU, Z., et al. Novel polarization-reconfigurable converter based on multilayer frequency-selective surfaces. *Pro*ceedings of the IEEE, 2015, vol. 103, no. 7, p. 1057–1070. DOI: 10.1109/JPROC.2015.2437611
- [37] KARAMIRAD, M., GHOBADI, C., NOURINIA, J., et al. Metasurfaces for wideband and efficient polarization rotation. *IEEE Transactions on Antennas and Propagation*, 2021, vol. 69, no. 3, p. 1799–1804. DOI: 10.1109/TAP.2020.3012828
- [38] CHENG, H., WEI, X., YU, P., et al. Integrating polarization conversion and nearly perfect absorption with multifunctional metasurfaces. *Applied Physics Letters*, 2017, vol. 110, p. 171903–171907. DOI: 10.1063/1.4982240
- [39] GHOSH, S., GHOSH, J., SANTOSHKUMAR SINGH, M., et al. A low-profile multifunctional metasurface reflector for multiband polarization transformation. *IEEE Transactions on Circuits* and Systems II: Express Briefs, 2023, vol. 70, no. 1, p. 76–80. DOI: 10.1109/TCSII.2022.3202085
- [40] SHIRZAD, H., GHOBADI, C., NOURINIA, J., et al. Single layer multi-band transmissive type linear to circular polarization converter with wide angular stability for C-, X-, and Kuband applications. *IEEE Access*, 2024, vol. 12, p. 14083–14093. DOI: 10.1109/ACCESS.2024.3355197
- [41] DUTTA, R., GHOSH, J., YANG, Z., et al. Multi-band multifunctional metasurface-based reflective polarization converter for linear and circular polarizations. *IEEE Access*, 2021, vol. 9, p. 152738– 152748. DOI: 10.1109/ACCESS.2021.3128190
- [42] KAYA, Y., HASAR, U. C., OZTURK, H., et al. Multi-functional, multi-band, low-profile, ultra-thin, and cost-effective metasurfacebased polarization converter. *Measurement*, 2025, vol. 248, p. 1–13. DOI: 10.1016/j.measurement.2025.116894
- [43] LI, Z., YANG, R., WANG, J., et al. Multifunctional metasurface for broadband absorption, linear and circular polarization conversions. *Optical Materials Express*, 2021, vol. 11, no. 10, p. 3507–3517. DOI: 10.1364/OME.437474
- [44] SINGH, V., BHATTACHARYYA, S., AGRAHARI, R., et al. A low-profile tri-functional metasurface toward polarization conversions and absorption. *IEEE Antennas and Wireless Propagation Letters*, 2024, vol. 23, no. 9, p. 2593–2597. DOI: 10.1109/LAWP.2024.3400375
- [45] PENG, L., LI, X., JIANG, X., et al. A novel THz half-wave polarization converter for cross-polarization conversions of both linear and circular polarizations and polarization conversion ratio regulating by graphene. *IEEE Journal of Lightwave Technology*, 2018, vol. 36, no. 19, p. 4250–4258. DOI: 10.1109/JLT.2018.2836904

#### **About the Authors...**

Sylvie RANA (corresponding author) was born in 1996 in India. She received her M.Tech. from Department of Electronics and Telecommunications, Indian Institute of Engineering Science and Technology (IIEST), Shibpur, India in 2021 and her B.Tech. from Maulana Abul Kalam Azad University of Technology (MAKAUT), West Bengal, India in 2018. She is currently pursuing her Ph.D. from the Indian Institute of Technology (IIT), Kanpur, India. Her research interests include anomalous reflection and transmission from phase gradient surfaces, reconfigurable intelligent surfaces, polarization converter, polarization selective absorber using metasurfaces etc. She is actively involved in various IEEE activities and recipient of two best paper awards for her contributions on IEEE Space Aerospace and DefenCE (SPACE) 2024 and IEEE Microwave Antenna and Communication (MAC) 2024 conferences.

Samiran PRAMANIK received his B.Tech. and M.Tech. degrees in Electronics and Communication Engineering from WBUT and Burdwan University, respectively, and his Ph.D. in Microwave Engineering from NIT Mizoram in 2024. Since 2010, he has been with the College of Engineering and Management, Kolaghat, where he is currently an Assistant Professor in the ECE department. His research interests include metasurfaces, polarization converters, absorbers, MIMO, radar, and RCS imaging. He has published over 15 papers in international journals and conferences.

Debasis MITRA received his B.E. in Electronics and Telecommunication Engineering from Bengal Engineering College (DU), M.Tech. in RF and Microwave Engineering from IIT Kharagpur, and Ph.D. from IIEST Shibpur. He is currently an Associate Professor in the Dept. of Electronics and Telecommunication, Indian Institute of Engineering Science and Technology, Shibpur, India. His research interests include metamaterials, microwave systems for healthcare, wireless power transfer, and frequency selective surfaces for radar applications. He has authored over 120 journal and conference papers. Dr. Mitra received the Visvesvaraya Young Faculty Fellowship (MeitY, GoI) in 2016 and the Young Faculty Research Award from the Global Alumni Association of BESU in 2018. He serves as a reviewer for journals such as IEEE AWPL, TAP, MTT, and IET MAP, and is a Senior Regional Editor for the Advanced Electromagnetics journal. He is currently leading several national and international projects funded by DBT, DST, SPARC-II, and DBT-Vinnova.

Chaitali KOLEY was born in West Bengal, India, in 1985. She received her Ph.D. degree in Electronics and Communication Engineering (Specialization: Microwaves) from the University of Burdwan. She is currently working as an assistant professor in the Electronics and Communication Engineering Department, National Institute of Technology Mizoram. Her research interests are in microwave communication and microwave oscillators. She has published more than 50 research papers in reputed journals and conferences. She has completed two projects and has one ongoing project.